Yang, L., *et al.*: Numerical Simulation and Optimization of Steel Tube Billet ...
THERMAL SCIENCE: Year 2023, Vol. 27, No. 5B, pp. 4179-4192

4179

NUMERICAL SIMULATION AND OPTIMIZATION OF STEEL TUBE BILLET HEATING PROCESS IN ROTARY HEARTH FURNACE USING COMPUTATIONAL FLUID DYNAMICS

by

Likun YANG[a], Fuyong SU[a], Zhi WEN[a], Shuming TAO[b], Guangjie BAI[c], and Chunmei LUAN[c]*

[a] School of Energy and Environmental Engineering,
University of Science and Technology Beijing, Beijing, China
[b] Baoshan Iron and Steel Co., Ltd., Shanghai, China
[c] Yantai Lubao Steel Pipe Co., Ltd., Yantai, China

Billet reheating is an important part of the steel production process. Since the production process will adopt different tube billet arrangement strategies, and the condition of the furnace hearth will also change due to long-term operation and accumulation of iron oxide scales, these factors will inevitably affect heating efficiency and temperature distribution uniformity of the tube billet, thereby affecting the quality of the final product. In this study, a physical and mathematical model was established for a 48 m diameter rotary hearth furnace of the seamless steel pipe production-line and typical 300 mm diameter tube billets of different lengths. Commercial FLUENT code was used to carry out CFD numerical simulation research on the influence of the aforementioned factors. Optimizing and adjusting strategies under different arrangement strategies were proposed, and the influence of furnace hearth condition change on heating effect was studied. The methods and simulation approach of this paper also have guidance for the billet heating control in similar continuous heating furnaces.

Key words: *rotary hearth furnace, tube billet heating, distribution angle,*
CFD numerical simulation, arrangement strategy,
furnace hearth condition

Introduction

Rotary hearth furnace (RHF) is an important equipment on the seamless steel pipe hot rolling production-line [1-3] It is mainly used for reheating the tube billets before perforation process. Due to its advantages of large capacity, good thermal uniformity, low unit fuel consumption and easy automation, it has been widely used since the 1960's and has become the main furnace type for billet reheating, and the structure design is becoming larger and larger. The equipment condition and operation level of the RHF directly affect the heating quality of the tube billets, which in turn affects the quality of the seamless steel tube. While heating efficiency directly affect the cost of steel pipes. With requirements getting higher and higher for the quality and diversification of seamless steel pipes from social production and manufacturing,

---

the popular computer optimization control of RHF based on CFD numerical simulation method gets more attention.

Many works of numerical simulation for RHF can be found from existing publications and most of them are the researches about metallurgical dust or pellet recycling application and usage [4-9]. Only a few of them are the discussions about steel billet heating. For instance, Blanco *et al.* [2] presented a mathematical model of the heating of round billets and used explicit and implicit finite difference method to solve heat transfer equations. Liu *et al.* [10] developed a 3-D mathematical model for simulation of flow, temperature, and concentration fields by using CFD method. Landfahrer *et al.* [11] also used CFD to develop a numerically highly efficient model, different combustion models were analyzed and compared. While DellaRocca *et al.* [12] presented an advanced CFD methods for the furnace, they evaluated the effects of regenerative burner flame on the billet reheating. Hadala *et al.* [13] modeled the charge heating process, the finite element method was applied.

But when it comes to the billet heating process, many more numerical simulation works still focus on various continuous heating furnaces except RHF [14-22], though RHF is one of the continuous types. Emadi *et al.* [20] performed an overall modelling and simulation of billets in a walking hearth type reheating furnace and got heating characteristics affected by various radiation. Gu *et al.* [21] conducted numerical simulation of slab heating process in a regenerative walking beam reheating furnace, a simplified method is described to study the slab heating process.

Unlike other continuous heating furnace types, RHF has hearth on which grooves are evenly distributed, and there's fixed angle between every two grooves. In the actual production process, different distribution angles will be used to arrange the tube billets intervals. Meanwhile, due to the fixed limited furnace width, different side-by-side distribution strategies will be used for tube billets with various lengths, such as single-row distribution for typical long tubes, and cross-distribution or double-row distribution for typical short billets. Some of the related studies based on similar continuous heating furnaces and square billets were carried out. Li *et al.* [23] predicted optimum values of square billet space in walking beam furnace. Monte-Carlo method was introduced to determine view-factor matrix of the furnace enclosure. Wu *et al.* [24] found that the addition of piers and alteration of square billet spacing can affect the heating performance in a batch-type furnace CFD case study. Most of the publications investigate conventional walking beam type and pusher type reheating furnaces, rare studies carried out based on RHF or tube billet production.

In RHF, adjustable flame burners are distributed on both sides of the furnace wall, and the shape of the adjustable flame will also affect the heating effect (uniformity of temperature distribution on the surface of the tube billets). When the flame length is fixed, there should be ideal heating conditions for different billets arrangement strategies. In order to find the specific rules or properties, numerical simulation of steel tube billet heating process in RHF will be carried out by using CFD.

Physical model description

Computational model simplification

The study is based on RHF in Yantai Lubao Steel Pipe Co., Ltd. (wholly-owned subsidiary of Baoshan Iron and Steel Co., Ltd.). The furnace has a central diameter of 48000 mm, an outer diameter of 55462 mm, the width of furnace hearth is 5600 mm. It adopts a flat-top structure, with seven temperature control (heating) zones and one heat recovery zone. These eight zones from billets discharging door to charging door are: Soaking II, Soaking I,

Yang, L., *et al.*: Numerical Simulation and Optimization of Steel Tube Billet ...
THERMAL SCIENCE: Year 2023, Vol. 27, No. 5B, pp. 4179-4192

4181

Heating III, Heating II, Heating I, Preheating II, Preheating I, and the heat recovery, as shown in fig. 1.

The evenly distributed grooves with fixed angle are arranged in the hearth of furnace, which can be shown by the center cross-section view in fig. 2.
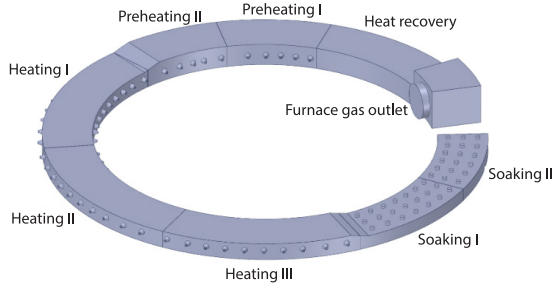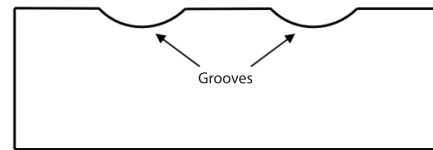

Figure 1. Schematic of RHF

Figure 2. The center cross-section view of furnace hearth

Due to the existence of the grooves, various uniform arrangement strategies of tube billets can be adopted in the production process. That's so-called distribution angle, as shown in fig. 3.

The distribution angle of the annular heating furnace is usually required to meet the expression:

$$(360° - \beta) = (N-1)\alpha \qquad (1)$$

where N is the current number of tube billets supported in the furnace. The fixed position of charging and discharging is required, and the selected distribution angle should not only

Figure 3. Distribution angle diagram;
α – distribution angle,
β – the discharging door angle range,
D – RHF central diameter,
1 – centre line of the discharging door, and
2 – centre line of the discharging door

meet the aforementioned expression, but also require that the angle β must be divisible by the angle α, so that a complete rotation of the furnace hearth and the process of billets charging/discharging can be done. The typical arrangement strategies used in routine production are shown in tab. 1. The distribution angle of this RHF is adjustable from 1.2°-2.5°, and the angle between the charging line and the discharging line is 12°.

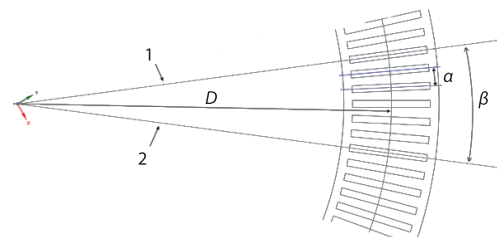**Table 1. Typical arrangement strategies of RHF**

Billet diameter [mm]	Number of grooves	Distribution angle [°]	Billet number supported	Interval number between adjacent billets
300	540	1.3333	261	1
380	540	1.3333	261	1
450	540	2	174	2

Due to the existence of the grooves, the part of the billets nearing the bottom of the grooves will not be easily heated, thus increasing the distribution angle should make a relatively good heating effect, and achieve better consistency of the temperature distribution and oxide formation. The specific effects will be revealed through follow-up studies.

Mathematical model

What takes place in the RHF is a complex process of flow, combustion and heat transfer. Describing these processes requires different governing equations. The turbulence model in simulation by ANSYS FLUENT code was based on standard k-ε. The governing equations in this paper include:

– Continuity equation

$$\frac{\partial}{\partial x_i}(\rho u_i) = 0 \tag{2}$$

– Momentum equation

$$\frac{\partial}{\partial t}(\rho \vec{u}_i) + \frac{\partial}{\partial x_i}(\rho \vec{u}_i \vec{u}_j) = -\frac{\partial p}{\partial x_i} + \frac{\partial \tau_{ij}}{\partial c_j} + \rho g_i + \vec{F}_i \tag{3}$$

– The k-equation:

$$\frac{\partial(\rho k u_i)}{\partial x_i} = \frac{\partial}{\partial x_j}\left[\left(\mu + \frac{\mu_t}{\sigma_k}\right)\frac{\partial k}{\partial x_j}\right] + G_k + G_b - \rho\varepsilon \tag{4}$$

– The ε-equation:

$$\frac{\partial(\rho\varepsilon u_i)}{\partial x_i} = \frac{\partial}{\partial x_j}\left[\left(\mu + \frac{\mu_t}{\sigma_\varepsilon}\right)\frac{\partial\varepsilon}{\partial x_j}\right] + C_{1\varepsilon}\frac{\varepsilon}{k}(G_k + C_{3\varepsilon}G_b) - C_{2\varepsilon}\rho\frac{\varepsilon^2}{k} \tag{5}$$

– Species transport equations:

$$\frac{\partial \rho u_j Y_i}{\partial x_j} = \frac{\partial}{\partial x_j}\left[\left(\rho D_{i,\mathrm{m}} + \frac{\mu_t}{\mathrm{Sc}_t}\right)\frac{\partial Y_i}{\partial x_j}\right] + R_i \tag{6}$$

– Energy equation

$$\frac{\partial}{\partial x_i}\left[u_i(\rho E + p)\right] = \frac{\partial}{\partial x_j}\left[\left(k + \frac{c_p \mu_t}{\mathrm{Pr}_t}\right)\frac{\partial T}{\partial x_j} + u_i \mu_{\mathrm{eff}}\left(\frac{\partial u_j}{\partial x_i} + \frac{\partial u_i}{\partial x_j} - \frac{2\partial u_1}{3x_1}\delta_{ij}\right)\right] + S_{\mathrm{chem}} + S_{\mathrm{rad}} \tag{7}$$

where

$$\tau_{ij} = \mu\left(\frac{\partial u_i}{\partial x_j} + \frac{\partial u_j}{\partial x_i}\right) - \frac{2}{3}\mu\frac{\partial u_l}{\partial x_l}\delta_{ij}, \quad \mu_{\mathrm{eff}} = \mu + \mu_t, \quad \mu_t = \rho C\mu\frac{k^2}{\varepsilon}, \quad C_{1\varepsilon} = 1.44$$

$$C_{2\varepsilon} = 1.92, \quad C_\varepsilon = 0.09, \quad \sigma_k = 1.0, \quad \sigma_\varepsilon = 1.3$$

$$G_k = \left[\mu_t\left(\frac{\partial u}{\partial x_j} + \frac{\partial u_j}{\partial x_i}\right) - \frac{2}{3}\left(\rho k + \mu_t\frac{\partial u_l}{\partial x_l}\right)\delta_{ij}\right]\frac{\partial u_j}{\partial x_i}, \quad G_b = \xi g_j\frac{\mu_t}{\mathrm{Pr}_t}\frac{\partial T}{\partial x_i}$$

Combustion and radiation model

The combustion method in this paper is the diffusion combustion of natural gas and air, so the non-premixed combustion probability density function (PDF) model is used in FLUENT code. This model does not solve the transport equation of a single component, but solves the transport equation of the mixed component distribution, and the concentration of each component is obtained from the mixed component distribution. The model assumes that the chemical reaction is fast enough that the reaction is dominated by the mixing rate. The PDF model obtains the composition and temperature fields by solving the transport equation for the mixture fraction and its variance. The governing equations are:

$$\frac{\partial}{\partial t}\left(\rho \overline{f}\right) + \nabla\left(\rho \vec{v}\overline{f}\right) = \nabla\left(\frac{\mu_t}{\sigma_t}\nabla \overline{f}\right) + s_m + s_{\text{user}} \tag{8}$$

$$\frac{\partial}{\partial t}\left(\rho \overline{f}'^2\right) + \nabla\left(\rho \vec{v}\overline{f}'^2\right) = \nabla\left(\frac{\mu_t}{\sigma_t}\nabla \overline{f}'^2\right) + C_g \mu_t \left(\nabla^2 \overline{f}\right) - C_d \rho \frac{\varepsilon}{k}\overline{f}'^2 + s_{\text{user}} \tag{9}$$

where

$$\overline{f}' = f - \overline{f}, \; f = \frac{Z_k - Z_{k,0}}{Z_{k,F} - Z_{k,0}}$$

In the combustion process in this paper, there are radiation participating mediums in the combustion products, the discrete ordinates (DO) radiation model is used:

$$\frac{dI(\vec{r},\vec{s})}{ds} + (a + \sigma_s)I(\vec{r},\vec{s}) = an^2 \frac{\sigma T^4}{\pi} + \frac{\sigma_s}{4\pi}\int_0^{4\pi} I(\vec{r},\vec{s}'')\Phi(\vec{s},s)(\vec{s},\vec{s}')d\Omega' \tag{10}$$

Combustion will produce a large amount of CO_2 and H_2O when using natural gas or mixed gas as fuel. Therefore, the combustion products have a great influence on the radiative heat transfer in the furnace. In order to simulate the effect of combustion products on the radiation in the furnace, its radiation and absorption coefficients need to be calculated. The weighted-sum-of-gray-gas model model was adopted for better accurate solution.

The RHF tube billets heating optimization

### *Computational model simplification and boundary conditions*

The physical model of the whole furnace includes the tube billets and the adjustable burners. Since the original model is very large, the size of the entire furnace body is very different from the minimum unit size (*e.g.*, the diameter of air inlet in adjustable burner is 20 mm), and in the previous simulation calculation of the flame-adjusted burner in the heating section, the flame shape of the over-detailed structure and the simplified structure were compared, and it was found that high similarity between flames of two structures could be achieved when using same burning condition. Therefore, it was decided to simplify the burner in the case study about billet reheating. Appropriate simplification of the model reduces the workload of simulation calculations, and correspondingly improves the calculation stability, so that accurate results can be obtained faster.

Before the case study, a routine black box heating experiment (using thermocouples) was conducted by field engineers on production-line. The experiment was carried out for a 4200 mm length and 300 mm diameter tube billet with grade of 29 Mn^2, the complete temperature curve of whole heating process was obtained. The 14 thermocouple points and relevant burying settings are shown in fig. 4. Hollow point means deeper burying depth (280 mm) while solid point means shallower burying depth (109 mm) which also made the couples directly contact atmosphere. Type *k* thermocouple with Class 1 accuracy was used for the experiment.

Though billet heating is a process with many ever-changing characteristics, in the studies for which we usually using transient simulation. But considering the aim of heating effectiveness study led by various billet arrangement strategies and furnace hearth condition change, and the heating curve which can be seen in fig. 5 from 107 minutes to 137 minutes in the graph (time of the black box experiment). We can see the furnace temperature is basically stable but the billet is still heating up significantly in the heating Zone II, so the initial part of heating Zone II (the part with the fastest temperature rising of the billet, until the temperature
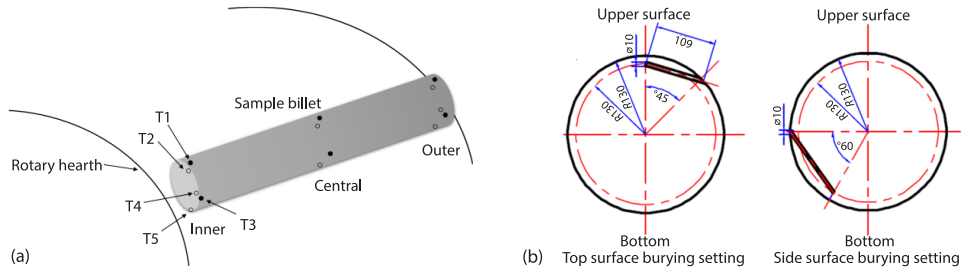
Figure 4. The black box heating experiment and specific burying settings of thermocouples; (a) rotary heath and (b) upper surface
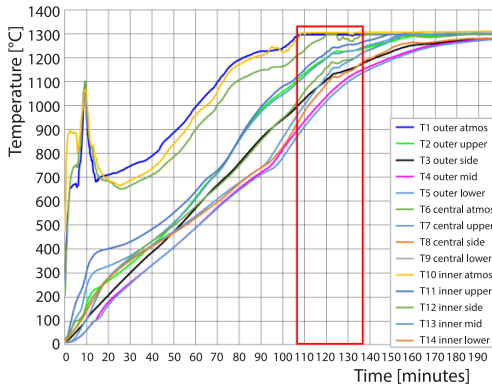
Figure 5. The heating temperature curve of the ∅ 300 mm × 4200 mm tube billet (the red frame area indicates the heating Zone II)
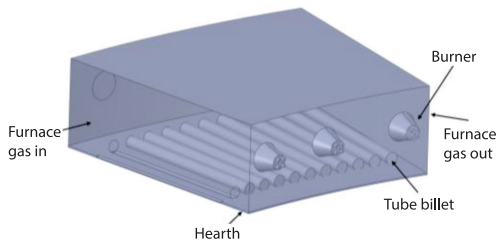
Figure 6. Heating Zone II with simplified burner structure and ∅ 300 × 4200 tube billets (α = 1.2°)

of the furnace gas from the middle test ring is stable in 120 minutes) could be selected instead of all heating zones as study object. Thus, the steady-state simulation method could be used instead of transient calculation, which can reflect the facts and greatly reduce the modelling, meshing and subsequent calculations workload. Meanwhile the ∅ = 300 mm tube billet is selected as study object, and the conclusions obtained can also be applied to the billets with other typical specifications, as shown in fig. 6. Referring to the thermocouple data, the regional inlet gas temperature can be uniformly set to 1300 °C, the pressure inlet is 32 Pa (provided by field data collection), the regional outlet temperature is 1280 °C, the pressure outlet is 30 Pa, the initial bottom surface temperature is 1273.15 K, and the initial temperature of the tube billets is 1173.15 K.

Natural gas was used for burner, detailed fuel chemical components are listed in tab. 2.

Table 2. Chemical components of fuel

Fuel type	Natural gas							
Component	CH_4	N_2	CO_2	C_2H_6	C_3H_8	C_4H_{10}	C_5H_{12}	C_{6+}
Mass Percentage [%]	93.508	1.011	1.046	3.503	0.603	0.203	0.061	0.065
Heating value [Kcalm^{-3}]	8450							

Yang, L., *et al.*: Numerical Simulation and Optimization of Steel Tube Billet ...
THERMAL SCIENCE: Year 2023, Vol. 27, No. 5B, pp. 4179-4192

4185

Hexahedral structured meshing method was used for the burner and tube billet parts, and tetrahedral unstructured meshing method for the rest of the zone (fluid area and the furnace hearth). In order to ensure high calculation accuracy and calculation efficiency, the mesh quantity was controlled at the million level. As shown in fig. 7, mesh was established with 250804 nodes and 877915 mesh cells. The constant wall temperature from T9 temperature in fig. 5 was set as the boundary condition of hearth. No-slip adiabatic wall was set as the boundary condition of side walls and roof.

Figure 7. Meshing of burner and billet parts

The SIMPLE algorithm was adopted for pressure-velocity coupling. The second-order central difference scheme was used to spatially discretize the governing equations of convection term and diffusion term. The calculation residuals was set to 10^{-6}.

At the mean time, a simulation of whole furnace was established to validate the model. T9 temperature from black box experiment, fig. 5, was set as furnace hearth constant value, no-slip adiabatic wall was set as the boundary condition of side walls and roof. A $z = 1300$ mm level surface (mounting height of side burners) temperature contour was obtained. The central temperature data values from simulation were

Figure 8 . Temperature contour of whole RHF ($z = 1300$ mm surface)

very close to the T6 temperature of fig. 5, error range was 5-10% approximately, which indicated the settings and models adopted by the simulations are reasonable.

Results and discussion

Discussion when distribution angle changes

Models were established by change distribution angle from $\alpha = 1.2°$ (the minimum) to $\alpha = 1.2666°$, $\alpha = 1.3333°$ (currently used), $\alpha = 1.4°$, and $\alpha = 1.4666°$. The surface heat flux density was recorded for comparative analysis, and the influence law of the change of the distribution angle in the typical state on the heating of the tube billet was obtained.

Excluding the influence of the air-flow at the inlet and outlet at the left and right ends of the model, select tube billet in the mid for data sampling. Because the top of the tube billet is close to the burner flame, it is directly facing the flame, the top thermocouple data/simulation data from the black box experiment/CFD simulation both show that the temperature is significantly higher than that of the horizontal middle level of the tube billet surface, so it is not suitable to use the top surface for data sampling. The bottom level of tube is too close to the hearth, it is hardly to see the temperature differences among multiple instances, they are far not as significant as the horizontal middle level of the tube billet, and it is also not suitable for use. Therefore, a linear data strip was taken on the horizontal middle level of the tube billet surface for analysis, as shown in fig. 8 (the yellow strip).
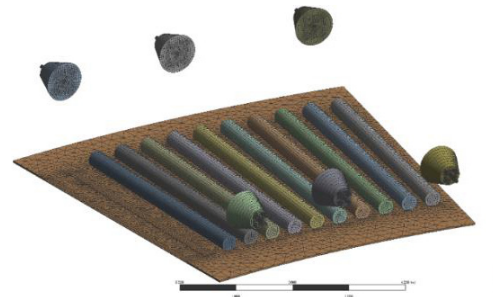
4186

Yang, L., *et al.*: Numerical Simulation and Optimization of Steel Tube Billet ...
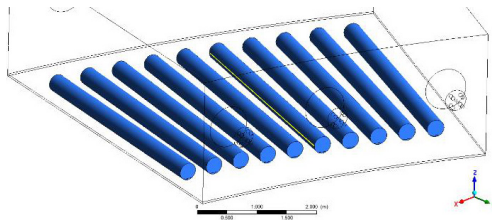THERMAL SCIENCE: Year 2023, Vol. 27, No. 5B, pp. 4179-4192

Figure 9. Data points indication

The contour of the surface heat flux density distribution could be obtained through the simulation, as shown in fig. 10.

Because of high data level, only very small difference could be noticed by the visual data from the contours even when comparing between $\alpha = 1.2°$ and $\alpha = 1.4666°$ samples shown in fig. 9, but when put all five sets of data in a dot-line graph and take the average and we could get comparisons more intuitively in fig. 11.
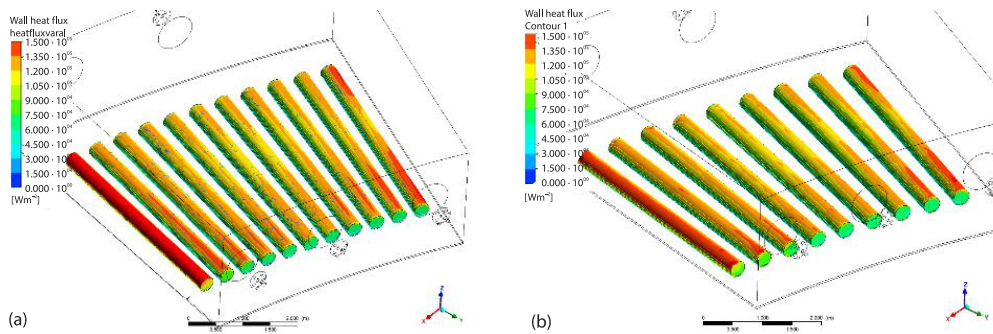

Figure 10. Surface heat flux density distribution contour result sample; (a) $\alpha = 1.2°$ and (b) $\alpha = 1.4666°$
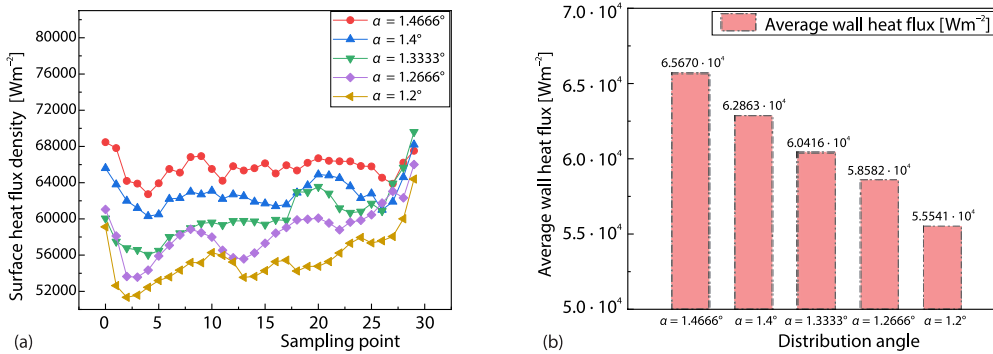

Figure 11. Comparison of surface heat flux density distribution and average values along linear sampling data strips under different distribution angles; (a) sampling point and (b) distribution angle

It can be seen that in the range of $\alpha = 1.2°$ to $\alpha = 1.4666°$, the surface heat flux density increases significantly with the increase of the distribution angle, and the average value of the data band can better reflect its regularity. The gradual increasing rate goes from 3-5%. Obviously, within the applicable angle range of the RHF, larger angle can bring higher heating efficiency to the tube billets.

*Discussion of effects by changing spacing between adjacent
rows of billets when using double-row distribution strategy*

The double-row distribution strategy can significantly increase the billets charging rate and increase the effective heat exchange area of the billet, shown in fig. 12. However, under the premise of a fixed flame length, the difference of the spacing between adjacent rows of billets will have an impact on the heating effect of the billet.

This section takes billets with a diameter of 300 mm and a length of 2250 mm as example. Within the allowable placement range of the length of the hearth, there are five different types of $d = 200$ mm, $d = 300$ mm, $d = 400$ mm, $d = 500$ mm, and $d = 600$ mm. The relative position (spacing) was used as a variable, and all the remaining boundary conditions are kept the same. When the 2250 mm tube billet is selected and the spacing of 600 mm is set, the distal ends of the two side-by-side tube billets are close to the edge of the hearth. The spacing is reduced in steps of 100 mm, and when the spacing is set to 200 mm, it is significantly smaller than the pipe diameter, so these five spacings were selected as variables.

Since the top of the tube billets is directly facing the flame and the high temperature flue gas, the relative position of the billets and the flame varies with the spacing d, the heating effect has been significantly changed. The effect can also be clearly seen from the contours in fig. 13. Therefore, a linear data strip was taken in the middle of the top surface of the billet, and 30 monitoring points were assigned. Figure 14 shows the data collected from the points.
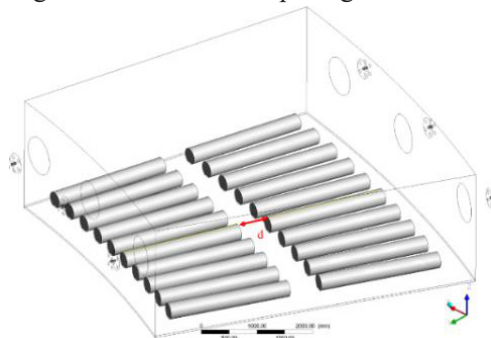

Figure 12. Schematic diagram of radial spacing between adjacent tube billets side by side when using double-row distribution strategy
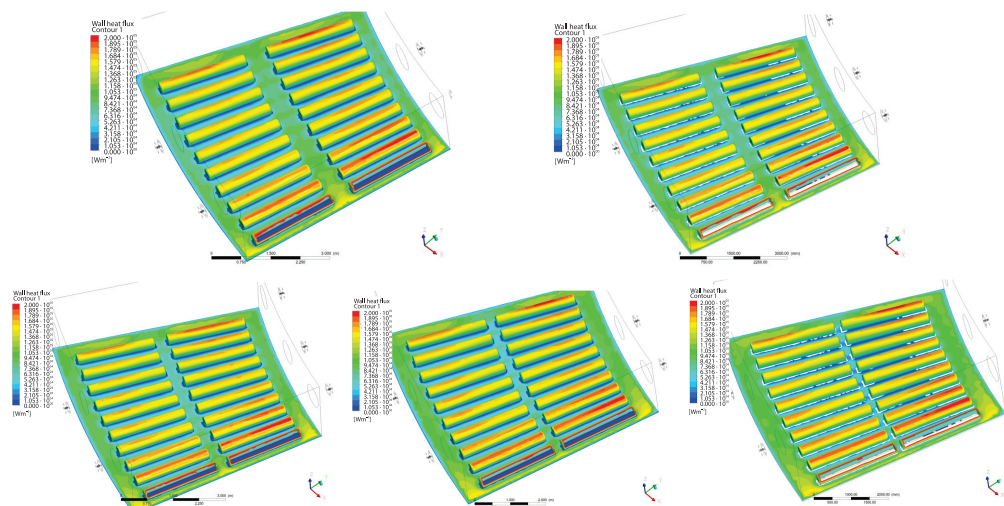
**Figure 13. Surface heat flux density distribution contours
(from left to right, top to bottom: $d = 600$ mm to $d = 200$ mm)**

Due to the constant flame length and the position change of the billet, the surface heat flux density distribution is significantly affected. When the spacing $d = 200$ mm, the high value

section of the heat flow density distribution heated along the direction of the billet has shifted significantly. This will result in uneven temperature distribution, which does not meet the ideal heating. It's ideal when the spacing d = 600 mm. When taking the average value of the surface heat flux distribution, it can be seen from fig. 14(b) that although there is a gradually increasing trend when spacing changes from 600-200 mm, the difference is very small (3.4% difference between the maximum and minimum cases), so it can be considered that the overall heating efficiency is at the same level and is minimally affected by spacing change.
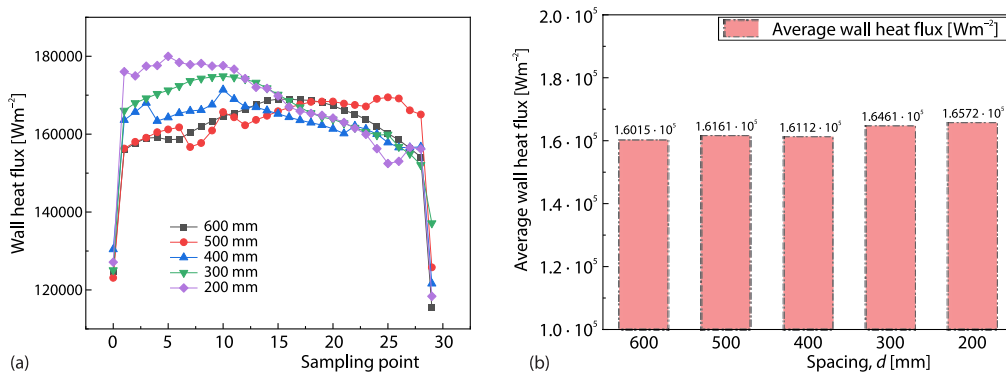
Figure 14. Comparison of surface heat flux density distribution and average values along the linear sampling data strip under different spacing when using double-row distribution strategy; (a) sampling point and (b) spacing d

We will get a clearer picture of this if we look at the temperature contours of the area, as shown in fig. 15(a) perspective contour of flame and billet, and 15(b) vertical view of flames. Therefore, it is best to adjust billets according to the flame shape under the current working conditions to ensure a more symmetrical and uniform temperature distribution of the billets.
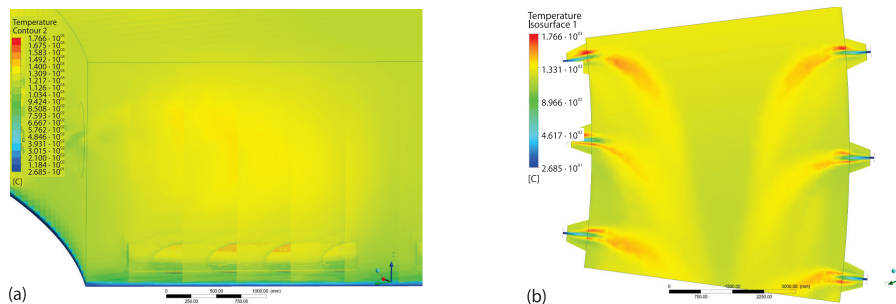
Figure 15. Contours of temperature distribution (d = 600mm); (a) perspective contour of flame and billet and (b) vertical view of flames

Discussion of effects when the furnace hearth condition changes

Due to the long-term operation of the furnace, the falling of iron oxide scales, fig. 16, and dust accumulation will cause a certain thickness of soft sedimentary layer to cover the hearth. Due to the huge weight, the tube billets will dig into the layer and get some of the bottom part buried, which in turn affects the heating of the tube billets. This section aims to study this influencing factor. As shown in fig. 17, $\varnothing$ 300 mm × 4200 mm tube and a fixed α = 1.3333° were selected. The tube billets buried depth is shown in h. In order to facilitate

Yang, L., *et al.*: Numerical Simulation and Optimization of Steel Tube Billet ...
THERMAL SCIENCE: Year 2023, Vol. 27, No. 5B, pp. 4179-4192

4189

modelling and maintain a high level of mesh quality, 10 mm depth was added to the hearth model, $h = 25$ mm was set as normal state. Around this, set $h = 15$ mm, $h = 20$ mm, $h = 30$ mm, and $h = 35$ mm for a total of five instances for simulation.

(a)   (b)   (c)

**Figure 16. Iron oxide scales dropped from billets and hearth photo taken through charging door**

The data sampling in this section focuses on the area instead of the stripes. Due to the obvious difference in the burying depth among five instances, there will be obvious difference in the areas exposed to the furnace gas either. The radiation and convection heat transfer of the covered part in the bottom should be significantly weakened, which should reduce the heating efficiency of the billets. Therefore, total heat transfer rate was used as a characterization parameter for comparison.

The simulation data of five instances were combined, as shown in fig. 18.
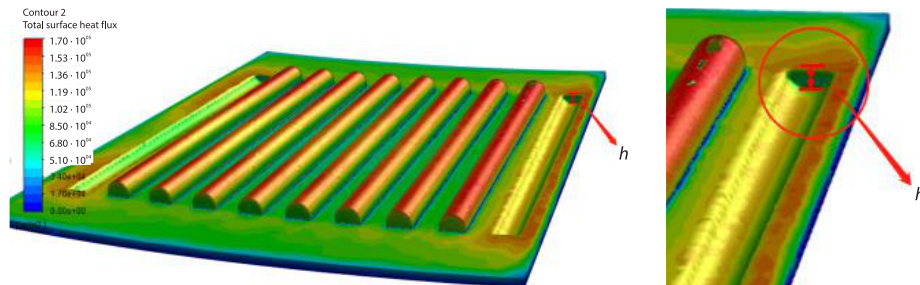
Figure 17. Schematic of billet burying depth

The results showed the efficiency drop clearly, which is consistent with the previous speculations. Although the selected heating part has the fastest heating rate in the entire process (Heating II), and the temperatures of the hearth and tube billets in other zone of are not the same, it should show a similar result, as long as the billets is kept in heating state. Therefore, more attention should be paid to the accumulation of iron oxide scales and dust during long-term production.
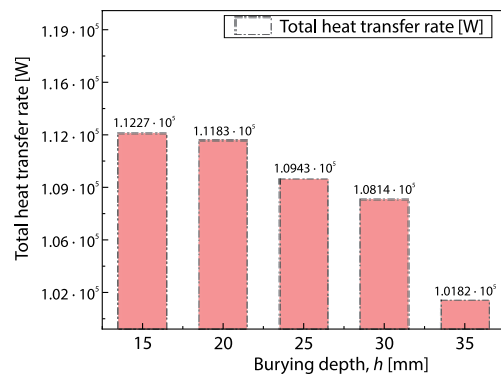
Figure 18. Comparison of total heat transfer rate of billet areas exposed to the furnace gas

Conclusions

A simplified CFD model of RHF is developed for studies on key problems in the routine tube billet reheating process. The simplification work is based on reasonable assumptions, which is suitable for qualitative research and engineering verification and greatly reduces the modelling and calculation workload, correspondingly improves the calculation stability, accurate and convincing results can be obtained faster. Following summaries are the important conclusions got from the aforementioned analysis based on this model.

- It is found that within the applicable distribution angle α range of the Lubao RHF, the surface heat flux density of the tube billets increases significantly with the increase of the angle α, which means higher heating efficiency of the billets. The average value of the sampled data stripes can better reflect the regularity: when $\alpha = 1.2°$, the average surface heat flux density is 55540.73 W/m². With the increase of α, the average surface heat flux density increased to 58582.46 W/m² ($\alpha = 1.2666°$), 60415.77 W/m² ($\alpha = 1.3333°$), 62863.33 W/m² ($\alpha = 1.4°$), 65669.83 W/m² ($\alpha = 1.4666°$), with a gradual increase of 3-5%.
- The study of effects by changing spacing between adjacent rows of billets when using double-row distribution strategy is achieved. Through the analysis of the results, it was proposed that it is best to adjust billets according to the flame shape under the current working conditions to ensure a more symmetrical and uniform temperature distribution of the billets.
- Total heat transfer rate was used as a characterization parameter for comparison in the study of effects when the furnace hearth condition changes. The CFD results show a significant total heat transfer rate drop trend with the deepening of the burying depth in the range of $h = 15$ mm to $h = 35$ mm. It can drop from $1.1227 \cdot 10^5$ W ($h = 15$mm) to $1.0943 \cdot 10^5$ W ($h = 25$ mm), and then to $1.0182 \cdot 10^5$ W ($h = 35$ mm). The minimum drop is 0.3% from 15-20 mm, and the highest is 6.21% from 30-35 mm. The results showed the efficiency drop clearly, which is consistent with the previous speculations. Although the selected heating part has the fastest heating rate in the entire process (Heating II), and the temperatures of the hearth and tube billets in other zone of are not the same, it should show a similar result, as long as the billets is kept in heating state. Therefore, more attention should be paid to the accumulation of iron oxide scales and dust during long-term production.

Nomenclature

a – asorption coefficient for gas medium, [–]
$C_{1\varepsilon}$ – constant in standard k-ε model, [–]
$C_{2\varepsilon}$ – constant in standard k-ε model, [–]
$C_{3\varepsilon}$ – constant in standard k-ε model, [–]
C_μ – constant in standard k-ε model, [–]
c_p – specific heat, [Jkg^{-1}K^{-1}]
E – total energy per unit mass, [Jkg^{-1}]
G_b – production of turbulent kinetic
    energy by buoyancy, [Jm^{-3}s^{-1}]
G_k – production of turbulent kinetic energy
    by velocity gradient, [Jm^{-3}s^{-1}]
g_i – component of the gravitational
    vector in the ith direction, [ms^{-2}]
I – radiation intensity, which depends on
    position $\vec{r}$ and direction $\vec{s}$ [Wm^{-2}sr^{-1}]
k – turbulent kinetic energy, [m²s^{-2}]
N – current number of tube billets
    supported in RHF, [–]
n – refractive index, [–]

Pr_t – turbulent Prandtl number, [–]
p – pressure, [Pa]
R_i – volumetric rate of creation
    of species i, [molm^{-3}s^{-1}]
$\vec{r}$ – position vector, [m]
Sc_t – turbulent Schmidt number, [–]
S_{chem} – source term of heat of chemical
    reaction, [Jm^{-3}s^{-1}]
S_{rad} – source term of heat of radiation, [Jm^{-3}s^{-1}]
s – path length, [m]
$\vec{s}$ – direction vector, [m]
$\vec{s}'$ – scattering direction vector, [m]
T – local temperature, [K]
u_i – velocity components, [ms^{-1}]
Y_i – mass fraction of species i, [–]
Z_k – mass fraction of species k, [–]

Greek symbols

α – billet distribution angle in RHF, [°]

Yang, L., *et al.*: Numerical Simulation and Optimization of Steel Tube Billet ...
THERMAL SCIENCE: Year 2023, Vol. 27, No. 5B, pp. 4179-4192

4191

β – discharging door angle range in RHF, [°]
δ_{ij} – Kronecker delta, [–]
ε – dissipation rate of turbulent kinetic energy per unit mass, [m²s⁻³]
μ – molecular viscosity, [kgm⁻¹s⁻¹]
μ_{eff} – effective viscosity, [kgm–1s⁻¹]
μ_t – turbulent viscosity, [kgm⁻¹s⁻¹]
ζ – coefficient of thermal expansion, [–]
ρ – density, [kgm⁻³]

σ – Stefan–Boltzmann constant, [5.67 · 10⁻⁸Wm⁻²K⁻⁴]
σ_k – turbulent Prandtl number for k in standard k-ε model, [–]
σ_ε – turbulent Prandtl number for ε in standard k-ε model, [–]
σ_s – refraction coefficient, [–]
Φ – scattering phase functions, [–]
Ω^i – solid angle, [sr]

Acknowledgment

References

[1]   Bohm, J., Control and Monitoring of a Rotary-Hearth and a Walking-Beam Furnace in a Large Continuous Tube-Rolling Mill, *Steel Times, 205* (1977), 897

[2]   Blanco, E., *et al*. Mathematical Model of the Heating of Round Billets in a Rotary Hearth Furnace for the Production of Seamless Steel Tubes, *IFAC Proceedings Volumes*, *22* (1989), 11, pp. 161-166

[3]   I. H., et al., Automatic Control System of Billet Reheating Rotary Hearth Furnace, *Proceedings,* International Conference on Industrial Electronics, Control, Instrumentation, and Automation, San Diego, Cal., USA, 1992, pp. 1417-1421

[4]   Dasgupta, S., *et al*., A Computational Study on the Reduction Behavior of Iron Ore/Carbon Composite Pellets in Both Single and Multi-Layer Bed Rotary Hearth Furnace, *Metallurgical and Materials Transactions B, 51* (2020), 2, pp. 818-826

[5]   Wu, Y., *et al.*, Process Optimization of Metallurgical Dust Recycling by Direct Reduction in Rotary Hearth Furnace, *Powder Technology, 326* (2018), Feb., pp. 101-113

[6]   Wu, Y., *et al*., Modelling of Thermochemical Behavior in an Industrial-Scale Rotary Hearth Furnace for Metallurgical Dust Recycling, *Metallurgical and Materials Transactions B, 48* (2017), July, pp. 2403-2418

[7]   Yuan, P., *et al*., Study on the Formation of Direct Reduced Iron by Using Biomass as Reductants of Carbon Containing Pellets in RHF Process, *Energy*, *141* (2017), Dec., pp. 472-482

[8]   Mishra, S., Roy, G. G., Effect of Amount of Carbon on the Reduction Efficiency of Iron Ore-Coal Composite Pellets in Multi-Layer Bed Rotary Hearth Furnace (RHF), *Metallurgical and Materials Transactions B, 47* (2016), Apr., pp. 2347-2356

[9]   Liu, Y., *et al*., Numerical Investigation of the Effect of C/O Mole Ratio on the Performance of Rotary Hearth Furnace Using a Combined Model, *Metallurgical and Materials Transactions B*, *45* (2014), Aug., pp. 2370-2381

[10] Liu, Y., *et al*., The CFD Modelling of Flow, Temperature, and Concentration Fields in a Pilot-Scale Rotary Hearth Furnace, *Metallurgical and Materials Transactions B*, *45* (2014), Jan., pp. 251-261

[11] Landfahrer, M., *et al*., Development and Application of a Numerically Efficient Model Describing a Rotary Hearth Furnace Using CFD, *Energy*, *180* (2019), Aug., pp. 79-89

[12] DellaRocca, A., *et al*., Advanced Design Methods for Rotary Hearth Furnaces, *Steel Times International*, *36* (2012), B1

[13] Hadala, B., *et al*., Optimization of Long Charge Heating in a Rotary Furnace, *Archives of Metallurgy and Materials*, *66* (2021), 2, pp. 659-668

[14] Chang, J. H., et al., Development of a Roller Hearth Furnace Simulation Model and Performance Investigation, *International Journal of Heat and Mass Transfer*, *160* (2020), 120222

[15] Landfahrer, M., *et al*., *et al*., Characterization of the Temperature Distribution on Steel Tubes for Different Operating Conditions in a Reheating Furnace Using CFD and Three Different Measuring Methods, *Applied Thermal Engineering*, *133* (2018), Mar., pp. 39-48

[16] Mayr, B., *et al*., CFD Modelling and Performance Increase of a Pusher Type Reheating Furnace Using Oxy-Fuel Burners, *Energy Procedia*, *120* (2017), Aug., 462-468

[17] Mayr, B., *et al.*, CFD Analysis of a Pusher Type Reheating Furnace and the Billet Heating Characteristic, *Applied Thermal Engineering*, *115* (2017), Mar., pp. 986-994

[18] Prieler, R., *et al.*, Prediction of the Heating Characteristic of Billets in a Walking Hearth Type Reheating Furnace Using CFD, *International Journal of Heat and Mass Transfer*, *92* (2016), Jan., pp. 675-688

[19] Prieler, R., *et al.*, Numerical Analysis of the Transient Heating of Steel Billets and the Combustion Process Under Air-Fired and Oxygen Enriched Conditions, *Applied Thermal Engineering*, *103* (2016), June, pp. 252-263

[20] Emadi, A., *et al.*, Heating Characteristics of Billet in a Walking Hearth Type Reheating Furnace, *Applied Thermal Engineering*, *63* (2014), 1, pp. 396-405

[21] Gu, M., *et al.*, Numerical Simulation of Slab Heating Process in a Regenerative Walking Beam Reheating Furnace, *International Journal of Heat and Mass Transfer*, *76* (2014), Sept., pp. 405-410

[22] Singh, V. K., Talukdar, P., Comparisons of Different Heat Transfer Models of a Walking Beam Type Reheat Furnace, *International Communications in Heat and Mass Transfer*, *47* (2013), Oct., pp. 20-26

[23] Li, G., *et al.*, Optimum Study of Billet Space in Walking Beam Furnace, *Journal of Northeastern University (Natural Science)*, *33* (2012), 389

[24] Wu, B., *et al.*, CFD Analysis of Batch-Type Reheating Furnace With Regeneratve Burners, *Proceedings*, Heat Transfer Summer Conference, Jacksonville, Fla., USA, 2008, pp. 225-234